A LORENTZ FORCE TYPE SELF-BEARING MOTOR WITH NEW 4-POLE WINDING CONFIGURATION

Seung-Jong Kim
Tribology Research Center, Korea Institute of Science and Technology, Seoul, 136-791 Korea
sjongkim@kist.re.kr

Keisuke Abe
Chiba Precision Co., Ltd., Chiba, 273-0005 Japan
keisuke.abe@chibaprecision.com

Hideki Kanebako
Research & Development Center, Sankyo Seiki MFG. Co., Ltd., Suwa, Nagano, 391-0106 Japan
hideki.kanebako@sankyoseiki.co.jp

Yohji Okada
Dept. of Mechanical Eng., Ibaraki University, Hitachi, Ibaraki-Pref., 316-8511 Japan
okada@mech.ibaraki.ac.jp

Chong-Won Lee
Center for Noise and Vibration Control, KAIST, Science Town, Daejeon, 305-701 Korea
cwlee@novic.kaist.ac.kr

ABSTRACT
Aiming at small-size high-speed non-contact rotating machines, this paper proposes a Lorentz force type self-bearing motor, where a new four-pole winding configuration is used to make it function both as a synchronous permanent-magnet (PM) motor and as a magnetic bearing. Due to using Lorentz force, the proposed motor has some good points such as linearity of control force and high efficiency over conventional self-bearing motors. And compared with the previously developed 8-pole type, it is advantageous to a high-speed motor. Focusing on the feasibility of the proposed motor, this paper introduces a prototype that is manufactured in a radial and outer-rotor type and successfully run up to 12,600 rpm without contact. Static and dynamic characteristics of the prototype are examined.

INTRODUCTION
So far, various types of self-bearing motors that are functional combination of a motor and a magnetic bearing have been developed [1-4]. Compared with motors supported by separate magnetic bearings, they are compact and advantageous to small-size rotating machine such as artificial heart and hard disk drive. But, since most of them use a reluctance force for levitation, they have some difficulties in design and control. It is because the reluctance force is nonlinear and the complex distribution of flux in air gap and the flux saturation in core material should be considered. In addition, the demagnetization of thin permanent magnets can be another serious problem for long-term use. To avoid these difficulties, Lorentz force type self-bearing motors were proposed, in which the control force is directly proportional to control current and thick permanent magnet is allowable. Han and Lee [5] developed such a Lorentz force type self-bearing motor in which a disk-shape rotor was sandwiched between two stators and the rotor and the stators had eight-pole. They also proposed a demodulation scheme for self-bearing motors with the arbitrary numbers of poles and phases. However, the demodulation process was quite complicated. Another Lorentz force type self-bearing motor was developed by Okada, et al. [6]. It has an eight-pole rotor and a three-phase four-pole stator with six concentrated windings. Even if it showed high efficiency and good dynamic characteristics, it was applicable to only an eight-pole motor. But, the eight-pole type is inadequate to a small high-speed motor.

This paper proposes a Lorentz force type four-pole self-bearing motor with a peculiar pole arrangement. A prototype was made in radial and outer-rotor type, where a ring-shape rotor has four permanent magnets inside, while an inner stator has single layer of six concentrated windings. Active levitation control of the rotor is applied to only two radial motions, and the tilting and axial motions are passively stable, premised

on the radial stability. In experiment, the rotor was successfully levitated and stably run over 12,000 rpm. In this paper, we focus on the examination of static and dynamic performances of the prototype.

OPERATION PRINCIPLE

For rotation, the proposed self-bearing motor works just like a four-pole PM motor. Figure 1(a) shows the rotor with four permanent magnets and a pair of coils. When the currents flow in the coils as depicted in the figure, Lorentz force acting on each coil is generated clockwise. As the coils are fixed to the stator, these forces react to the rotor to produce a motor torque counterclockwise. The principle of the radial force generation is shown in Fig. 1(b). Compared with Fig. 1(a), the direction of current flow in a coil is opposite. That is, the currents in two coils are out of phase, which produces the radial resultant force as shown in Fig. 1(b). Note that the direction of this resultant force depends on the rotor angular position.

Extending Fig. 1 to the case of six three-phase coils is Fig. 2. Successive coils are positioned so that their magneto-motive-force (*mmf*) axes are at intervals of 60 degrees along the periphery. The entry and return paths of each coil are 90 degrees apart, equal to the interval of permanent magnets, which is to obtain maximum force

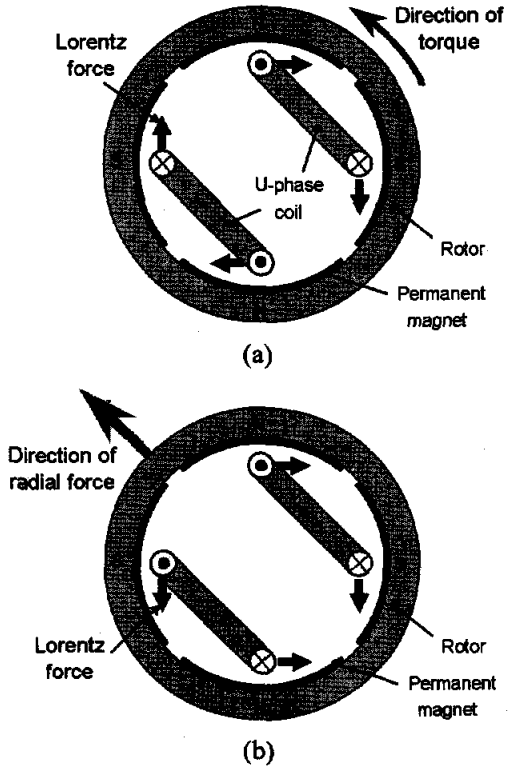

FIGURE 1: Principles of (a) the motor torque and (b) radial force generation

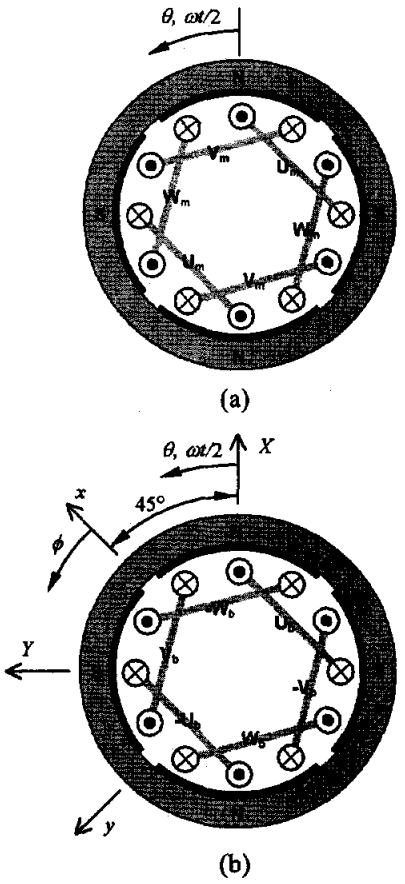

FIGURE 2: Phase currents arrangements for (a) motor torque and (b) radial force generations in the 4-pole self-bearing motor

and torque. For rotation, the three-phase currents should be arranged as U_m, V_m, W_m, U_m, V_m, W_m-phases in turn, as shown in Fig. 2(a), providing a traveling four-pole flux distribution. And for levitation, the arrangement of phase currents should be U_b, $-W_b$, V_b, $-U_b$, W_b, $-V_b$ -phases in turn, as shown in Fig. 2(b), providing a two-pole flux distribution. However, structurally their winding configurations are just the same. Thus, it is possible to use only a set of windings in common for rotation and levitation.

EXPERIMENTAL SETUP

Prototype

Figure 3 shows a prototype of the proposed self-bearing motor which is a radial and outer-rotor type, and its design parameters are listed in Table 1. The inner stator that is laminated with thin silicon-steel plates has twelve slots and six separate coils. Each coil is wound round three cores and holds a core in common with the adjacent coils. Using a stator with slots enables us to

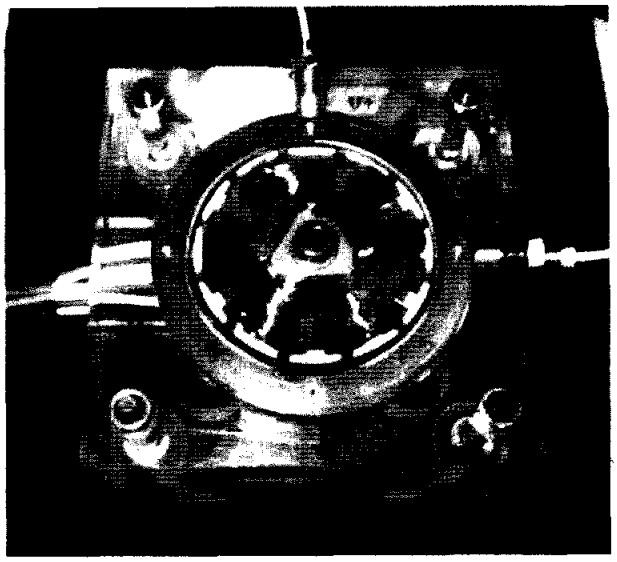

FIGURE 3: Prototype of the proposed self-bearing motor

TABLE 1: Design parameters of the prototype

Rotor			
Outer diameter	81 mm	Thickness of PM	1 mm
Inner diameter	65 mm	No. of PM	4
Thickness	10 mm	Rotor mass	135 g
Stator			
Diameter	60 mm	No. of slots	12
Thickness	10 mm	No. of coil turns	70
Air gap to PM	1.5 mm	Coil diameter	0.6 mm

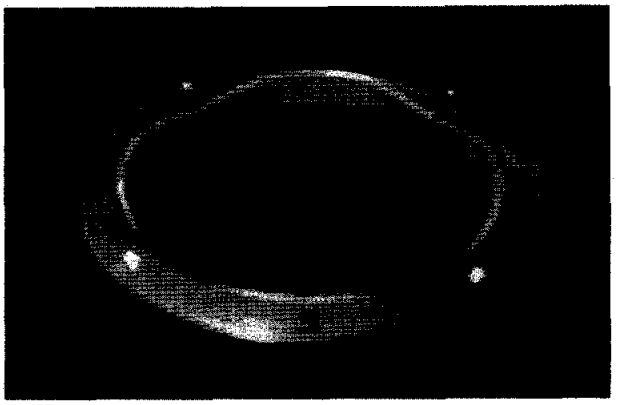

FIGURE 4: Rotor with four permanent magnets

increase the number of coil turns and shorten the air gap, which leads to relatively large Lorentz force. However, there is a trade-off that the attractive force destabilizing the rotor is also increased and the flux density saturation problem in cores revives. Here, note that the Lorentz force is determined from the flux density of air gap and the *mmf* of coils, whether coils are stuck on the slot-less stator surface or buried in slots [7].

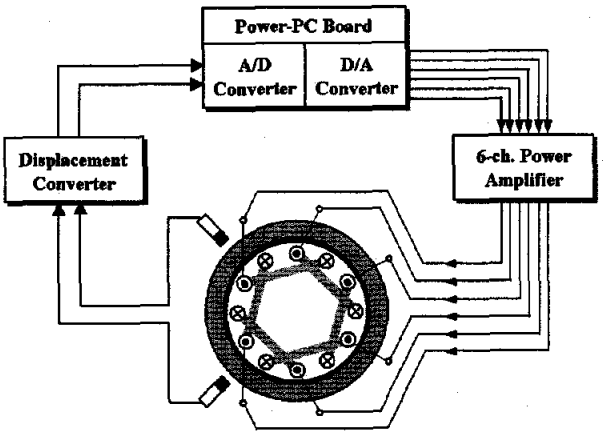

FIGURE 5: Schematic of the controlled system

On the other hand, the rotor shaped like a ring has four permanent magnets in the inner surface of it; two N poles and two S poles by turns, as shown in Fig. 4. The permanent magnets are diamond-shaped so that they can provide sinusoidal flux distribution circumferentially. Radial permissible displacement of the rotor is restricted to 0.5 mm by a touchdown base that is made of acrylic material. The radial displacement of the rotor is measured from the outside by two proximity probes built in the touchdown base.

Control system

Figure 5 shows a schematic signal flow of the control system, which consists of a self-bearing motor, two proximity probes, a host PC with a digital signal processor (dSPACE Inc., DS1103), and a linear power amplifier. Because six coils should be driven separately for rotation and levitation control, the power amplifier has six channels and its maximum current is ±5 A. For levitation control, radial displacements of rotor are measured and transferred into the control board of the host PC via a 16 bits A/D converter with sampling frequency of 10 kHz. And then, control signals are calculated in a standard PID controller for each direction. The control gains used in experiment are K_P= 1.1 and K_D = 0.0011, which were determined based on the measured system parameters such as sensor gain of 2.5 V/mm, amplifier gain of 1 A/V, and negative stiffness of the uncontrolled system. To transform the control signals to three-phase currents synchronized with the motor driving currents, we use

$$\begin{Bmatrix} I_{U_b} \\ I_{V_b} \\ I_{W_b} \end{Bmatrix} = \frac{2}{3}\begin{bmatrix} \cos\omega t & -\sin\omega t \\ \cos(\omega t + 2\pi/3) & -\sin(\omega t + 2\pi/3) \\ \cos(\omega t + 4\pi/3) & -\sin(\omega t + 4\pi/3) \end{bmatrix}\begin{Bmatrix} i_x \\ i_y \end{Bmatrix} \quad (1)$$

From these control signals and the motor driving currents, a set of self-bearing motor driving currents is

obtained as

$$I_{U_m}+I_{U_b}, I_{V_m}-I_{W_b}, I_{W_m}+I_{V_b}, I_{U_m}-I_{U_b}, I_{V_m}+I_{W_b}, I_{W_m}-I_{V_b}$$

in turn. Here, the motor driving currents are generated in the PC without rotational speed feedback. Its amplitude used in experiments was 2 A. Through the power amplifier, six currents calculated above flow into the respective coils to generate the torque and stabilize the levitation simultaneously.

EXPERIMENT

Static Magnetic Force and Torque

Prior to the experiment of levitation and rotation, the flux density in the air gap is measured, and the characteristics of static magnetic force and torque are examined. Figure 6 shows that as intended in the design of permanent magnets, the circumferential flux density distribution approximates well to a sine curve of $B(\theta) = -0.46\sin 2\theta$ except for some distortions caused by slots. It enables to separately control the torque and the levitation force [6]. Figure 7 shows the change of radial attractive force by permanent magnets according to the rotor displacement varied, where the slope of the approximate line is called as position stiffness. In the figure, it is examined about -25.5 N/mm. On the other hand, radial electromagnetic force measured with the current increased is shown in Fig. 8. Here the slope of the approximate line is defined as a current stiffness, which is about 3.3 N/A. In these cases, the rotor angle was fixed and the phase ϕ was set to produce the maximum force. The figures show good linear characteristics. Though the relation between force and displacement is actually not linear, Figure 7 shows that it doesn't matter to deem it linear within a narrow range.

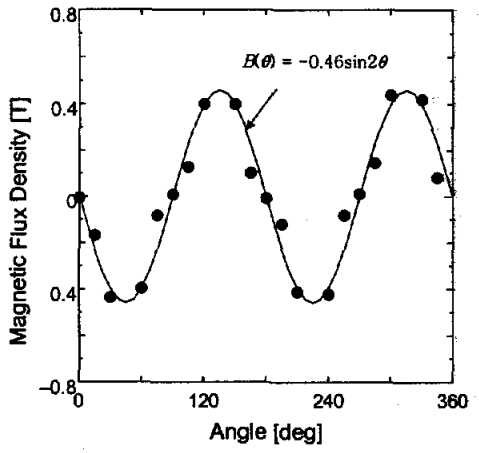

FIGURE 6: Flux density distribution measured in the air gap

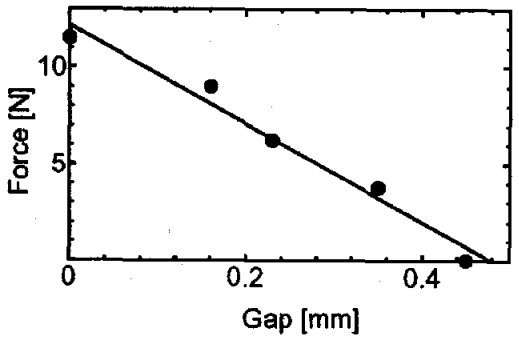

FIGURE 7: Position stiffness by permanent magnets

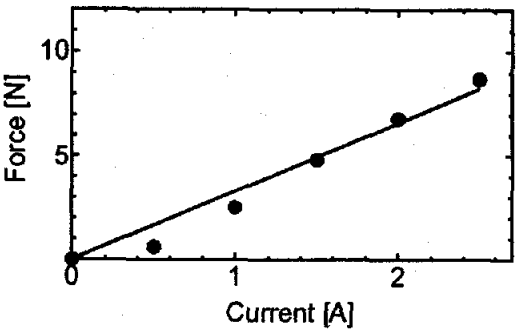

FIGURE 8: Current stiffness when the rotor is at center

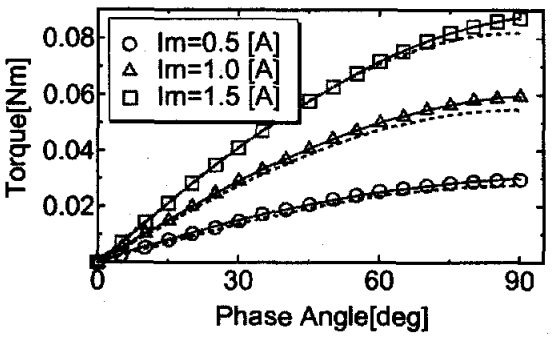

FIGURE 9: Static torque versus phase angle for motor currents of 0.5, 1.0 and 1.5 A

Figure 9 shows the characteristics of static torque, where each hidden line means the simulation result and symbols are the measured values. The measured and calculated results coincide well with each other. Here, for the simulation, the measured parameters such as the maximum flux density of Fig. 6 were used.

Levitation and Rotation Test

Figure 10 shows a time response of rotor when the levitation control starts at 0.2 sec. The rotor is very stably levitated and the residual vibration caused by a tilting motion is also damped out in 0.4 sec. To examine

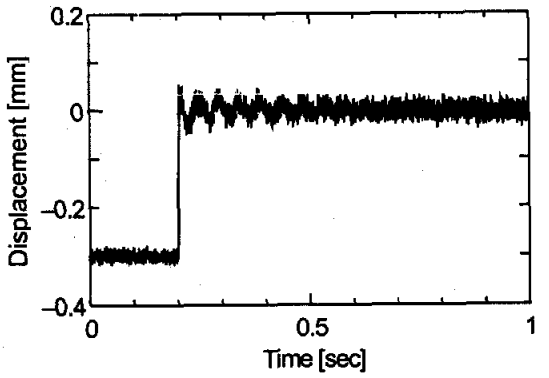

FIGURE 10: Start-up test in a radial direction

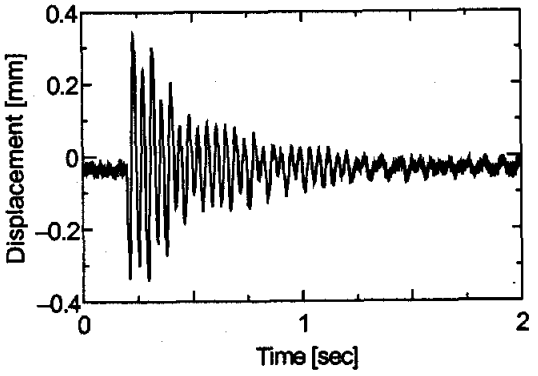

FIGURE 11: Impulse response in the axial direction: impacting at $\theta = 0°$ and measuring at 90°

the passive stability in axial and tilting motions, impact test was carried out. Figure 11 shows the impulse response in the case of impacting the rotor at $\theta = 0°$ and measuring at $\theta = 90°$ in axial direction. The signal consists dominantly of two frequency components: 12.6 Hz and 23.8 Hz, which are the tilting mode and the axial translation mode, respectively. Note that since those motions are passively stable, they have very low damping, which may affect the system stability. For reference, the natural frequency of radial motion is about 85 Hz.

In a speed-up test, the rotor could successfully rotate over 12,000 rpm as it was levitated. This test was done with the rotation axis fixed horizontally, so that the axial and tilting motions could be free from the gravity. Figure 12 shows the amplitudes of vibration, where Fig. 12(a) is for radial direction and Fig. 12(b) is for axial vibration. As predicted above, large axial and tilting vibrations appear at low rotational speed, and the radial vibration is reduced beyond the radial natural frequency of about 5,000 rpm. The maximum speed was 12,600 rpm, which was limited by the back electro-motive force (*emf*). Generally, PM motors produce high back *emf*. Figure 13 shows the change of back *emf* in the proposed motor according to the speed-up, which was

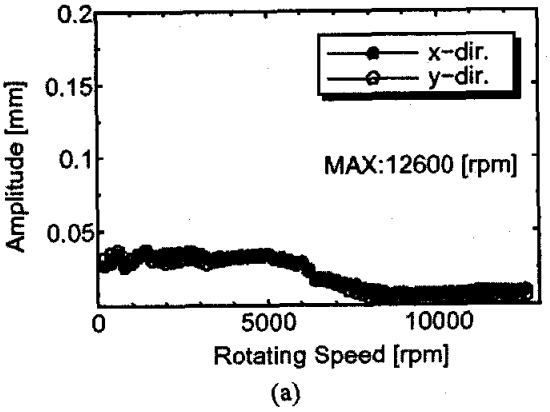

(a)

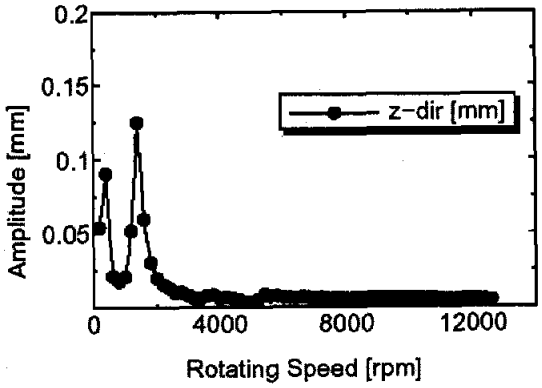

(b)

FIGURE 12: Amplitudes of (a) radial and (b) axial vibrations with the rotational speed increased

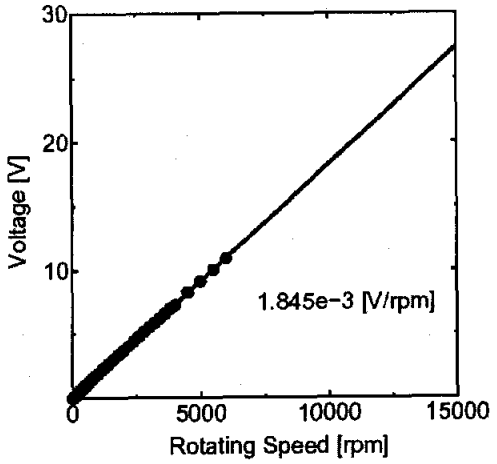

FIGURE 13: The measured back electro-motive force

measured with the rotor supported by a ball bearing and driven by an external DC motor. In the figure, the back *emf* is directly proportional to the rotational speed and comes near to the supply voltage (±24 V) of the power amplifier at 12,000 rpm.

On the other hand, dynamic torque was measured according to the rotational speed increased, as shown in

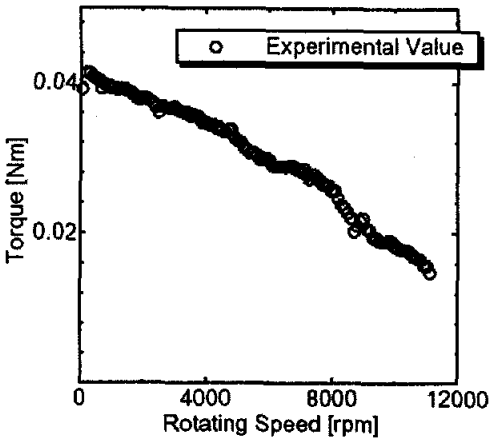

FIGURE 14: Dynamic torque

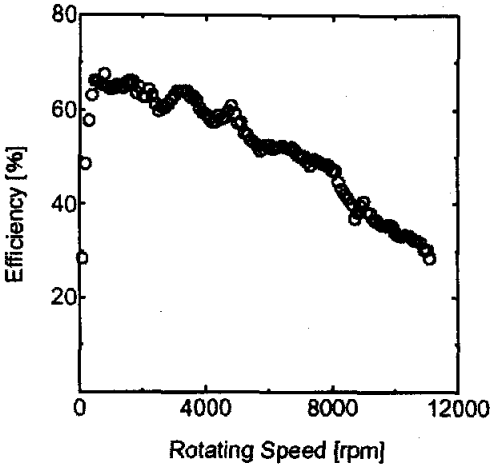

FIGURE 15: Motor efficiency

Fig. 14. During the test, the rotor was supported by two external ball bearings, and the levitation current was 0 A, while the amplitude of motor driving current was 1 A. In the figure, the maximum torque measures only about 70% of the static torque of Fig. 9, which is judged to be due to the loss of ball bearings and the error in setting up of a measurement device. And the decrease of the torque according to the speed-up is caused by the back *emf*. Figure 15 shows the motor efficiency, which is defined as

$$motor\ efficiency\ [\%] = \frac{motor\ output\ [W]}{motor\ input\ [W]} \qquad (2)$$

where

$$motor\ output\ [W] = 2\pi/60 \times torque\ [Nm] \times rotational\ speed\ [rpm] \qquad (3)$$

$$motor\ input\ [W] = I_{rms} V_{rms} \cos\frac{R}{\sqrt{R^2 + (\omega L)^2}} \qquad (4)$$

Here, I_{rms} and V_{rms} are the root-mean-square values of input current and voltage, respectively, ω is the rotational frequency, and R and L are the resistance and inductance of the coil, respectively. In the Fig. 15, the maximum efficiency measures 67%.

CONCLUSIONS

A Lorentz force type self-bearing motor with four poles was developed and the peculiar configuration of pole arrangement was proposed, which is very useful for a small high-speed rotating machine. To verify the proposed scheme, a prototype was made, where only the radial motions were actively controlled, while the tilting and axial motions are passively stable relying on the radial stability. The motor succeeded in very stable levitation and rotation over 12,000 rpm. The maximum speed that was limited by the back *emf* can be increased by using higher supply voltage. The experimental results showed the feasibility of the proposed self-bearing motor.

REFERENCES

1. Schöb, R. and Barletta, N., Principle and Application of a Bearing Slice Motor, Proc. of the 5th Int'l Symp. on Magnetic Bearings, Kanazawa, Japan, Aug. 1996, pp.313~318.
2. Chiba, A., Deido, T., Fukao, T. and Rahman, M. A., An Analysis of Bearingless AC Motors, IEEE Trans. on Energy Conversion, vol.9, no.1, 1994, pp.61~68.
3. Okada, Y., Miyamoto, S. and Ohishi, T., Levitation and Torque Control of Internal Permanent Magnet Type Bearingless Motor, IEEE Trans. on Control System Technology, vol.4, no.5, 1996, pp.565~571.
4. Kim, S. J., Shimonishi, T., Kanebako, H. and Okada, Y., Design of a Hybrid-type Short-span Self-bearing Motor, Proc. of the 7th Int'l Symp. on Magnetic Bearings, Zurich, Switzerland, Aug. 2000, pp. 359~364.
5. Han, W. S. and Lee, C. W., Runout Identification and Precision Control of Integrated Motor-Bearing System, Proc. of the 8th Int'l Congress on Sound and Vibration, Hong-Kong, China, 2001, pp. 1849~1856.
6. Okada, Y., Konishi, H., Kanebako, H. and Lee, C. W., Lorentz Force Type Self-bearing Motor, Proc. of the 7th Int'l Symp. on Magnetic Bearings, Zurich, Switzerland, Aug. 2000, pp. 353~358.
7. Say, M. G., Introduction to the unified theory of electromagnetic machines, 1st edition, Pitman Publishing, 1971.